X-661-72-36

NASA TM X-65825

A HIGH SENSITIVITY SEARCH FOR X-RAYS FROM SUPERNOVA REMNANTS IN AQUILA

D. A. SCHWARTZ
R. D. BLEACH
E. A. BOLDT
S. S. HOLT
P. J. SERLEMITSOS

FEBRUARY 1972

GSFC — GODDARD SPACE FLIGHT CENTER —
GREENBELT, MARYLAND

A HIGH SENSITIVITY SEARCH FOR X-RAYS FROM SUPERNOVA REMNANTS IN AQUILA

D. A. SCHWARTZ*, R. D. BLEACH**, E. A. BOLDT,
S. S. HOLT, and P. J. SERLEMITSOS

NASA/Goddard Space Flight Center
Greenbelt, Maryland

ABSTRACT

We have performed a high sensitivity scan of the galactic plane from ℓ = 70° to ℓ = 30° to search for 2-20 keV X-rays from supernova remnants. We report here on the spectra of five X-ray sources detected between 44° and 31° longitude, of which only two might be associated with suggested supernova remnants. Upper limits are presented for the 19 possible supernova remnants scanned in this survey.

*NAS-NRC Resident Research Associate
Present address: American Science and Engineering
Cambridge, Mass.

**Permanent Address: Dept. of Physics, University of Maryland
College Park, Md.

I. Experimental Configuration

Our detectors consisted of two multi-anode, multi-layer proportional counters (Holt et al., 1971), each with 2° x 8° FWHM rectangular collimators and 650 cm^2 net area. Both counters had 1 mil aluminized mylar windows, which defined an effective low energy threshold around 2 keV. One counter contained one atmosphere of argon, the other an atmosphere of xenon, and both had about 10 percent methane overpressure. We used 128 channel pulse height analyzers to cover the range 1.6 to 24 keV in the argon and 2 to 32 keV in the xenon detector. Table 1 gives the deduced normalization constants for a measured total count rate of 1.0 sec^{-1} within the energy band 2-10 keV from the top three layers of both detectors for incident spectra of power law $dN/dE = KE^{-n}$ photons $(cm^2 sec\ keV)^{-1}$ or exponential $dN/dE = K/E \exp(-E/kT)$ form, for several values of n or kT. The last column gives the corresponding energy flux in the 2 to 10 keV band. The total count rate, as a function of time, is compared with the aspect solution to derive positions and fluxes for the sources.

An Aerobee 170 carried these detectors to an altitude of 91 miles above the White Sands Missile Range on 1970 September 21. The aspect solution was determined by star field photographs obtained with two asynchronous cameras. Each took a three second exposure about every ten seconds. Based on the times of observation of Cyg X-1, Cyg X-2, and Cyg X-3, we made a correction of 0.2° to the pre-flight calibration photographs and we believe the final aspect solution is accurate to about 0.2°.

The data discussed here (Figure 1) span 65 seconds at the end of the flight. The background level was determined during the immediately preceding 44 seconds (Schwartz et al., 1971) as we scanned the galactic plane from 69° to 46°, observing no discrete sources above a 3σ limit of 0.02 photons $(cm^2 sec)^{-1}$ between 2 and 10 keV. We did not observe the source GX+48.7, reported above this limit in 1966 (Gursky et al., 1967). This background count rate agrees very well with the rate expected by folding the known diffuse X-ray spectrum through our detector response function and adding the internal detector background estimated from a previous flight when the detectors faced the earth.

The letters at the bottom of Figure 1 indicate events in the rocket attitude-control-system program. Figure 2 shows the detector scan path. The line A to B represents the end of a slow roll scan, $\sim$ 0.5°/sec, along the galactic plane. From B to C and C to D fast pitch and roll maneuvers occur. During the entire time from A to D the collimator is oriented very nearly perpendicular to the galactic plane, with the 2° resolution in galactic longitude. At D the rocket performs a clockwise 90° yaw maneuver, so that the 2° resolution is in galactic latitude during the final slow roll scan from D to E. The payload door closes at E, while atmospheric absorption is still negligible above 2 keV. Our multiple scans with different collimator orientations allow us to derive two dimensional positions for the sources between 30° and 40° longitude.

II. Analysis for Discrete Sources

Examination of Figure 1, compared to the detector scan path, shows that at least five distinct, discrete sources are observed: three at 296, 303, and 314 seconds during the scan in galactic latitude, another source between 282 and 291 seconds during the yaw maneuver, and a source around 252 seconds during the scan in longitude. It turns out that five sources suffice to explain all the count rates of Figure 1. The analysis proceeds by a (non-linear) least squares fit of the unknown source strengths and positions to the count rates measured over 0.2 second intervals. Accurate initial guesses were made by eyeball fitting of the detector's triangular response function to the data of Figure 1. Our final results, shown in Figure 2 and Table 2, give a χ^2 value of 342, for 324 data points. This solution depends on the following assumptions: we adopt the minimum number of sources necessary to fit the data, we assume the source strengths are constant in time, and we assume the source sizes are less than 0.2° so that they appear as point objects to our collimator.

The error boxes shown in Figure 2 generally represent a 2σ uncertainty. An exception is the source at 43.9° longitude, for which we do not have a latitude measurement. We have placed the center of this box on our scan circle, giving a minimum source strength, and used the 8° FWHM response angle for the latitude uncertainty.

Figure 2 also shows 19 non-thermal galactic radio sources suggested as supernova remnants (Milne, 1970; Downes, 1971). The actual radio size is shown for objects greater than 15' in diameter. Three of the X-ray sources are clearly <u>not</u> associated with any supernova remnant.

The third source in Table 2 can be identified with the non-thermal radio source 3C 396.1, and the fourth source can be identified with any of three suggested supernova remnants. In view of the large error boxes for the X-ray sources and the number of supernova remnants, these identifications are necessarily tentative. Note, however, that using more stringent requirements for identifying supernova remnants (Poveda and Woltjer, 1968) 3C 392 would be the only remnant in Figure 2, and a chance coincidence with an X-ray source would be much less likely.

III. Spectra

Our spectral data for the five sources are shown in Figures 3 and 4. We attempt to fit power law and exponential spectral parameters, as described for our observation of discrete X-ray sources in Cygnus (Bleach et al., 1972). Our two different detector gases, and the use of several layers within each detector give us checks against systematic errors in the spectral determination. The results are less precise than for the Cygnus sources because of the smaller count rates.

The best fit to source 1 is $dN/dE = .06E^{-.73}$. A χ^2 test gives an acceptable fit for indices in the range 0 to -2.3 and normalization constants between 0.04 and .23. A thermal spectrum of temperature hotter than kT=12 keV could also fit the data. Source 2 (Ser XR-1) cannot be fit by a power law. An exponential fit gives $dN/dE = (.42/E)\, e^{-E/7}$. The acceptable range of kT is 4.7 to 11.5 keV and the range of the normalization constant is 0.34 to 0.66. Source 3 can be fit by a power law $\frac{dN}{dE} = .24^{+.7}_{-.2} E^{-(1.9 \pm 1.0)}$ or by a thermal spectrum with a

temperature greater than 3 keV. For the remaining sources we can only make the qualitative spectral statements that number 4 is "hard" and 5 is "soft". Multiplying the energy flux column of Table 1, by the actual strength from Table 2 would give the energy flux for the source for any spectral shape.

IV. Discussion

In Table 3 we present upper limits to the X-ray flux from the 19 supernova remnants scanned. The upper limit count rate for each source is determined as the larger of either a 2σ increase above background or all the counts above background from points where the collimator response to the given source exceeds 20%. The upper limit naturally is higher for those remnants which fall near one of the five detected discrete sources. For the radio sources 3C 396.1, and 3C 392, or sources number 83 or 84 of Downes' (1971) catalog we may have a positive detection of X-rays at the flux levels given in Table 3, but the error boxes on the sources we have detected are too large to assert this with any certainty. In converting our count rates to photon fluxes we have assumed power law spectra for the sources, in agreement with the Crab, Tycho, and Cas A, the three supernova remnants previously detected as X-ray sources in the energy range above 2 keV. To convert to upper limits on the intrinsic X-ray luminosity we used the distances determined by Milne's (1970) empirical relation between intrinsic diameter and radio surfaces brightness at 1 GHz, for non-thermal galactic radio sources.

Our most likely detection of X-rays from a supernova remnant is the identification of our fourth source with 3C 392. First, from the

catalog of Poveda and Woltjer (1968), which contains only 26 objects selected to be supernova remnants by high reliability criteria, 3C 392 is the only remnant in the area of Figure 2. Second, the empirical results of Gorenstein, et al., (1970) suggest that hard X-rays might be expected from the more compact remnants, and 3C 392 has a radius of about 7 pc while that of 3C 396.1 is about 16 pc. The three known hard x-ray emitting supernova remnants, the Crab, Cas A, and Tycho, have radii in the range of about 1-4 pc, and intrinsic x-ray luminosities within an order of magnitude of each other. Examination of Table 3, however, indicates that any hard X-ray luminosity from either 3C 396.1 or 3C 392 must be at least two orders of magnitude below that of the Crab.

REFERENCES

Bleach, R. D., Boldt, E. A., Holt, S. S., Schwartz, D. A., Serlemitsos, P. J., 1972, Ap. J., 171, 51.

Downes, D., 1971, Astronomical Journal, 76, 305.

Friedman, H., Byram, E. T., and Chubb, T. A., 1967, Science, 156, 374.

Giacconi, R., Kellogg, E., Gorenstein, P., Gursky, H., and Tananbaum, H., 1971, Ap. J. (Letters), 165, L27.

Gorenstein, P., Gursky, H., Kellogg, E. M., and Giacconi, R., 1970, Ap. J., 160, 947.

Gursky, H., Gorenstein, P., and Giacconi, R., 1967, Ap. J. (Letters), 150, L75.

Holt, S. S., Boldt, E. A., Schwartz, D. S., Serlemitsos, P. J., and Bleach, R. D., 1971, Ap. J. (Letters), 166, L65.

Milne, D. K., 1970, Aust. J. Phys., 23, 425.

Poveda, A., Woltjer, L., 1968, Astronomical Journal, 73, 65.

Schwartz, D. A., Boldt, E. A., Holt, S. S., Serlemitsos, P. J., and Bleach, R. D., 1971, Nature, 233, 110.

TABLE 1

Detector Response vs. Spectral Shape

Spectrum (photons sec^{-1} cm^{-2} keV^{-1})	Shape Parameter	K*	Energy Flux* ergs $(cm^2\ sec)^{-1}$ 2-10 keV
$\frac{dN}{dE} = KE^{-n}$	n = 1.0	6.0×10^{-4}	7.7×10^{-12}
	n = 2.0	$30. \times 10^{-4}$	7.7×10^{-12}
	n = 3.0	$110. \times 10^{-4}$	7.0×10^{-12}
$\frac{dN}{dE} = \frac{K \exp (-E/kT)}{E}$	kT=2.0	6.4×10^{-3}	7.3×10^{-12}
	kT=5.0	1.9×10^{-3}	8.1×10^{-12}
	kT=10.0	1.1×10^{-3}	8.0×10^{-12}

*Assuming a measured 1.0 counts per second within the band 2-10 keV

Table 2

Discrete X-Ray Sources in Aquila

Source	b*	ℓ*	Strengths (counts sec^{-1})	Previous Identification
1	1.3	43.9	140	X1[1]
2	4.7	36.2	350	Ser XR-1[2], GX 36.3[3], W1[1]
3	-4.7	31.5	115	(Aql XR-1 ?)[2]
4	- .6	35.6	50	V1[1], (Aql XR-1 ?)[2]
5	-8.3	33.9	125	(Aql XR-1 ?)[2]

[1]Giacconi et al., 1971

[2]Friedman et al., 1967

[3]Gursky et al., 1967

*See figure 2 for positional errors.

Table 3

X-Ray Emission From Supernova Remnants

Designation[1]	ℓ	b	Radius[2] (pc)	Distance[2] (Kpc)	Upper Limits 2-10 keV X-Ray Flux counts/cm^{2}sec	Energy ergs/sec
D77,M63	29.7	-0.3	4.0	16.9	0.049	5×10^{36}
D78,M64	31.9	0.0	4.4	8.6	0.039	10^{36}
D79,M65,3C396.1	32.0	-4.9	15.8	1.8	0.061	7×10^{34}
D80,M66	33.1	0.0	8.6	3.4	0.030	10^{35}
D81,M67	33.7	0.0	6.5	7.1	0.038	7×10^{35}
D82,M68,3C392	34.6	-0.4	6.8	1.5	0.058	5×10^{34}
D83,M69	35.6	0.0	6.6	4.7	0.082	6×10^{35}
D84	35.6	-0.4	6.9	4.0	0.082	5×10^{35}
D85,M70	37.6	-0.1	9.4	2.2	0.069	10^{35}
D86,M71	39.2	-0.3	5.3	8.0	0.032	7×10^{35}
D87,M72	39.6	-1.8	11.8	1.6	0.046	4×10^{34}
D88,M73	41.1	-0.3	7.0	5.3	0.037	4×10^{35}
D89,M74	41.9	-4.1	15.0	0.7	0.069	10^{35}
D90,M75	43.3	-0.2	4.2	7.3	0.106	2×10^{36}
D91,M76	45.5	0.1	4.2	8.7	0.086	2×10^{36}
D92,M77	46.8	-0.3	6.4	5.8	0.038	5×10^{35}
D94,M78	47.6	6.1	17.4	2.0	0.050	7×10^{34}
D95,M79,W51	49.0	-0.3	6.4	1.9	0.019	2×10^{34}
D96,M80	53.6	-2.2	11.6	4.0	0.023	10^{35}
Crab Nebula	184.3	-6.2	1.0	2.0	2.2	10^{37}

[1]D = Downes (1971); M = Milne (1970)

[2]From Milne (1970)

FIGURE CAPTIONS

Figure 1 - Total count rate in top three layers of xenon and argon during the scan of Aquila. Dashed line indicates total background, as determined between 202 and 246 seconds after launch. The letters indicate events in the rocket scanning program, as discussed in the text.

Figure 2 - Shaded boxes and ellipse: X-ray sources detected in this experiment. Dots and open circles: suggested supernova remnants, with actual size of the radio source shown if greater than 15'. The solid line shows the track of the center of the collimators, and the letters denote events in the rocket aspect-control program, as described in text.

Figure 3 - Apparent flux from sources 1, 2, and 3. The data points represent the observed count rate divided by the nominal exposure and energy range, for the first layer of the xenon filled counter. No efficiency corrections have been made. The solid lines represent the best fit spectra folded through the complete detector response function. The best fits are $.06\ E^{-.73}$ for source 1, $\frac{.42}{E}\ EXP\ (-E/7.)$ for source 2, and $.24\ E^{-1.9}$ for source 3.

Figure 4 - Apparent flux from sources 4 and 5. The solid lines represent the best fit spectra, which are $.02\ E^{-.65}$ for source 4 and $.22\ E^{-1.9}$ for source 5.

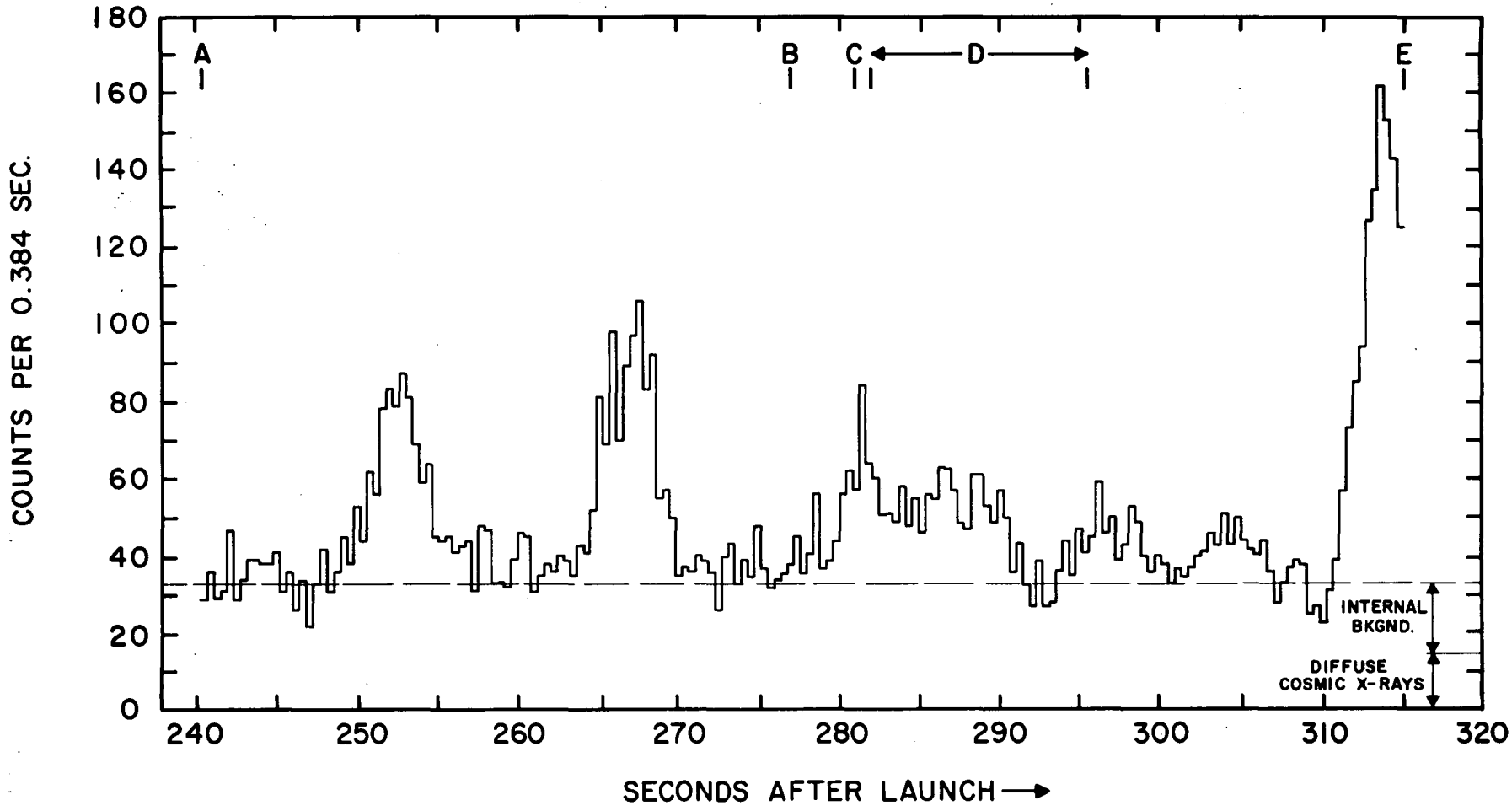
COUNTS PER 0.384 SEC.
180
160
140
120
100
80
60
40
20
0
A
B
C
D
E
INTERNAL BKGND.
DIFFUSE COSMIC X-RAYS
240
250
260
270
280
290
300
310
320
SECONDS AFTER LAUNCH

FIGURE 1

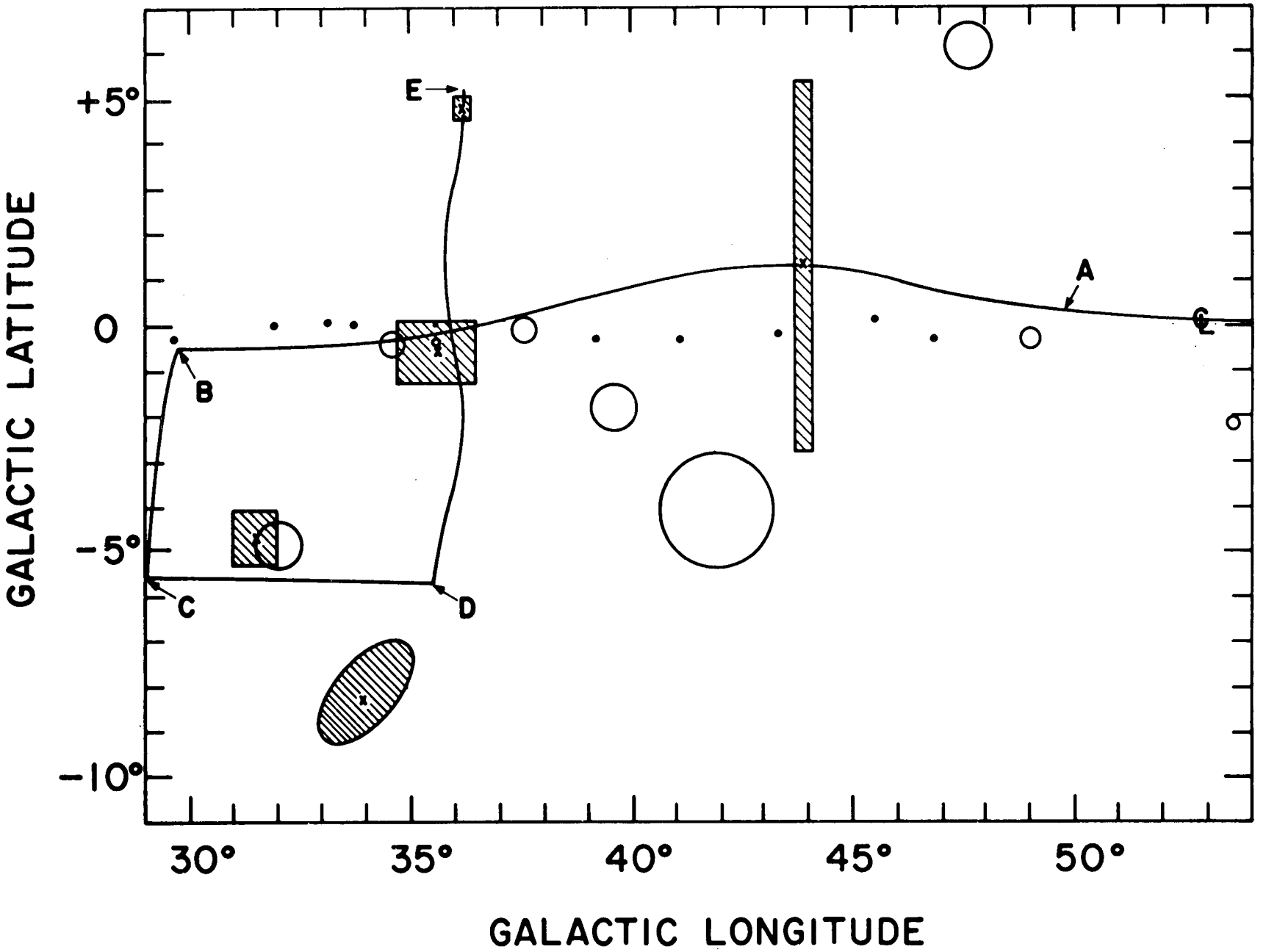
+5°
0
-5°
-10°
GALACTIC LATITUDE
30°
35°
40°
45°
50°
GALACTIC LONGITUDE
A
B
C
D
E

FIGURE 2

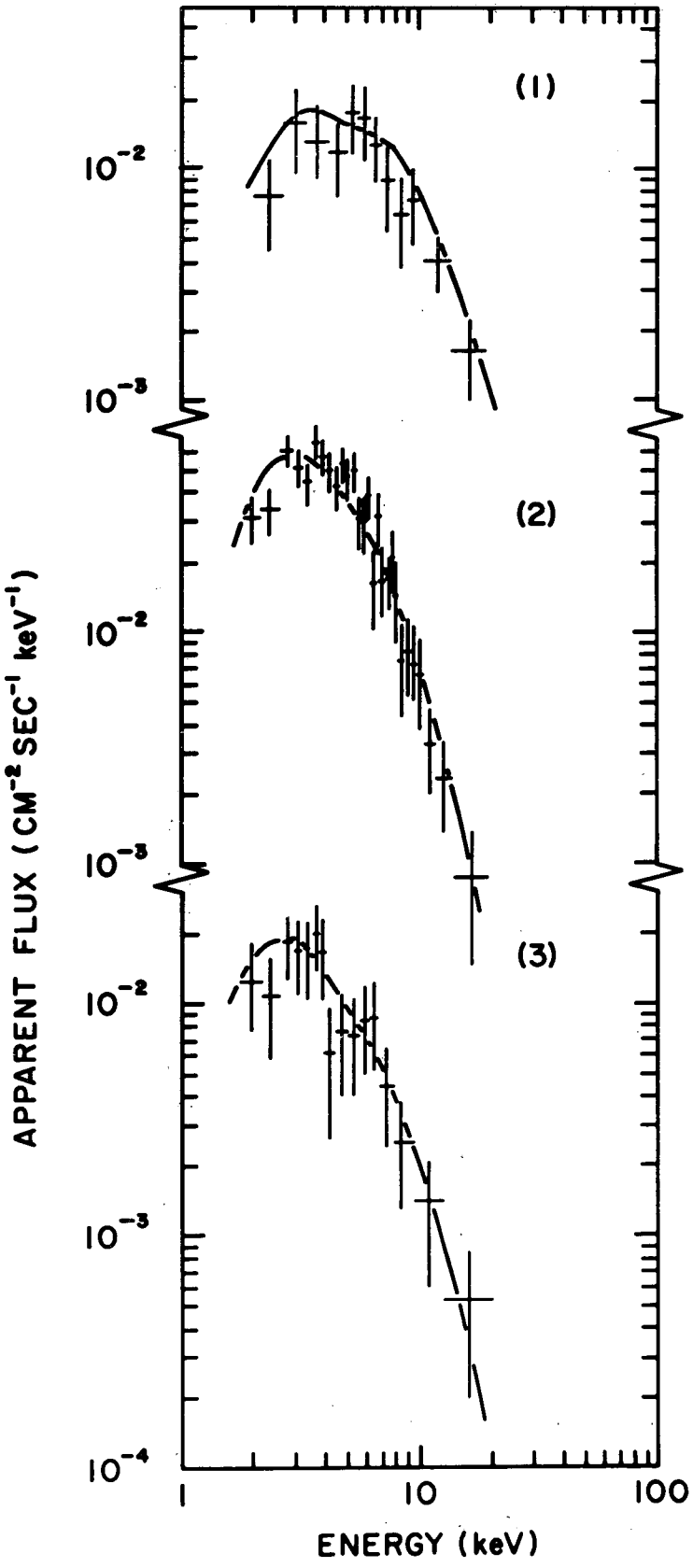
(1)
(2)
(3)
10^{-2}
10^{-3}
10^{-2}
10^{-3}
10^{-2}
10^{-3}
10^{-4}
APPARENT FLUX (CM^{-2} SEC^{-1} keV^{-1})
1
10
100
ENERGY (keV)

FIGURE 3

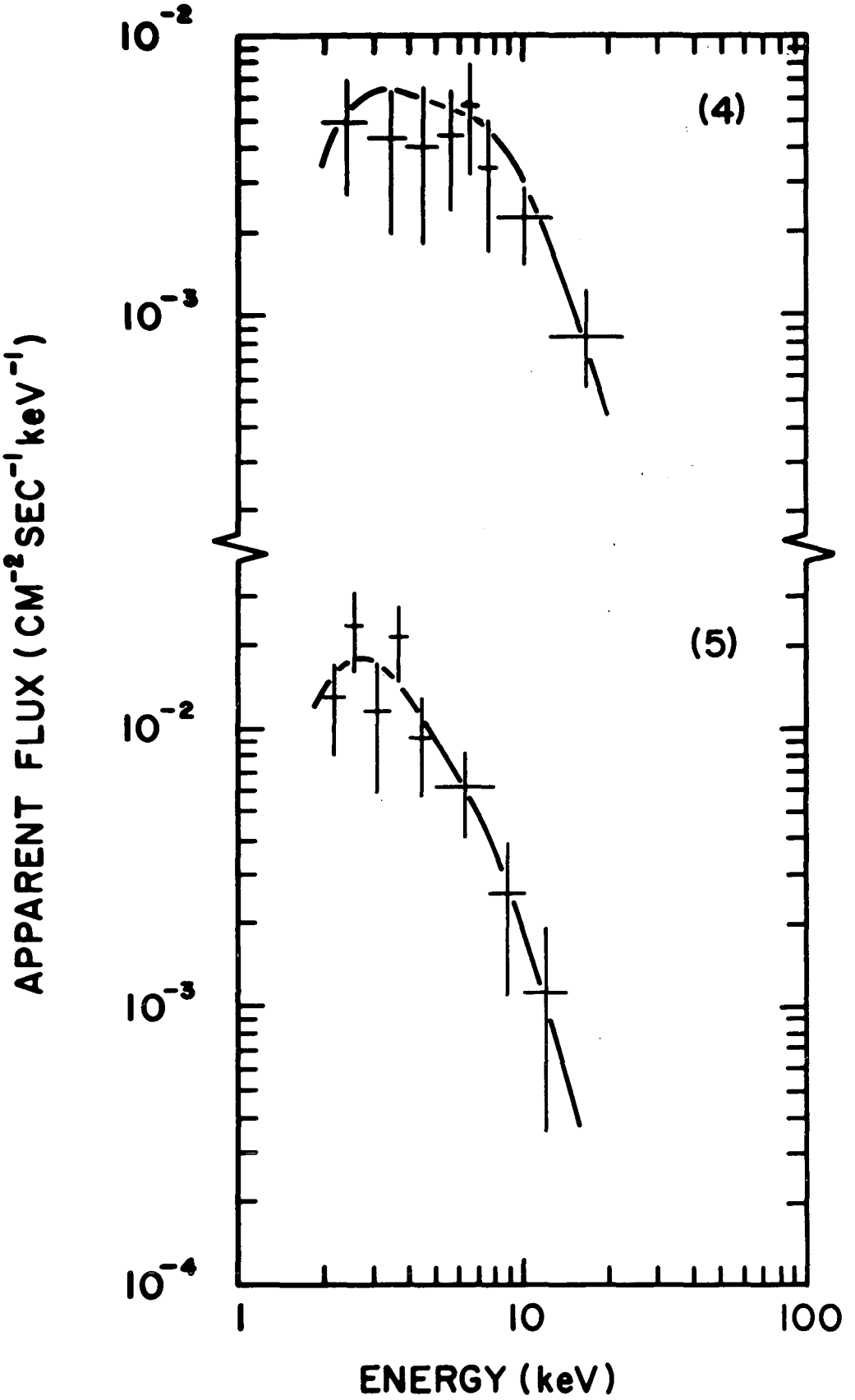
APPARENT FLUX (CM⁻²SEC⁻¹keV⁻¹)
10⁻²
10⁻³
10⁻²
10⁻³
10⁻⁴
(4)
(5)
1
10
100
ENERGY (keV)

FIGURE 4